Mechanics of Time-Dependent Materials
https://doi.org/10.1007/s11043-022-09572-x

Localized creep analysis of polyurea elastomer from full-field measurements

Nha Uyen Huynh[1] · Behrad Koohbor[2] · George Youssef[1]

Received: 1 June 2022 / Accepted: 11 October 2022

Abstract
Polyurea is an elastomeric polymer with segregated segmental microstructure and superior mechanical properties that are sensitive to loading time and temperature. In the research leading to this report, the primary goal was to elucidate the contributions of different segmental structures to the time-dependent creep deformation and material properties, such as Poisson's ratio and the creep modulus. The approach consisted of recording high-resolution digital images and resolving the full-field strain components of creep-loaded polyurea using digital image correlation (DIC) analysis. The resulting normal axial and lateral strains exemplified a typical creep response of incompressible elastomeric polymers, denoting the primary and secondary creep regions. Despite the uniaxial loading conditions, the presence of detectable shear strains demonstrated the occurrence of creep-activated shear softening behavior. The resolved strain contour maps, unique to DIC strain analysis, revealed noteworthy strain localization (demarked as striations on the strain contour plots) in selected regions within the observed regions of interest. The localized strains were separated and organized as functions of elapsed loading time. The high-strain regions were attributed to the soft segments of polyurea with inferior mechanical properties to their hard counterparts. The extracted time history of striations revealed three distinct molecular relaxation processes: one within primary creep attributed to the convoluted contributions of the hard/soft segmental microstructure and two processes within secondary creep associated independently with the hard and soft domains, respectively. The outcomes of this research are important for the development of effective and versatile polyurea-based impact-mitigating structures.

Keywords Polyurea · Creep analysis · Digital image correlation · Elastomeric polymers · Segmental microstructure

1 Introduction

The pursuit of effective and lightweight impact mitigation mechanisms gave rise to the emerging specific polyurea group of materials due to their hyperviscoelastic response, which

✉ G. Youssef
gyoussef@sdsu.edu

[1] Experimental Mechanics Laboratory, Mechanical Engineering Department, San Diego State University, 5500 Campanile Drive, San Diego, CA 92182, USA

[2] Department of Mechanical Engineering, Rowan University, 201 Mullica Hill Road, Glassboro, NJ 08028, USA

Published online: 26 October 2022

results in substantial strain energy dissipation. Polyurea, in different forms, e.g., bulk, thin films, microspheres, and foams (Do et al. 2020; Huynh et al. 2021; Raman et al. 2013; Reed et al. 2020; Roland et al. 2007; Wang et al. 2009), has been investigated for the protection of humans and critical assets against low-velocity and hypervelocity projectiles, respectively, in various operational and environmental conditions. The impact and shock tolerance of polyurea coatings and foams demonstrated superior energy dissipation response and effective protection of the underlying structures by reducing the severity of the incoming impact while altering the deformation mechanisms of the protective gear or armor plates (*e.g.*, plastic bulging versus fragmentation of polyurea-coated steel armors) (Gupta et al. 2015). In the above-mentioned studies, polyurea is a thermoset elastomer with segmental microstructure of soft aliphatic segment regions and hard aromatic segment domains (Hsieh et al. 2019). It is also worth noting that polyureas represent a broad material technology that can be formulated as linear polymers, i.e., thermoplastics (Sánchez-Ferrer et al. 2021, 2015), depending on the chemical structure of the constituents and the environmental conditions surrounding the preparation process. In general, the segmental structure is associated with different relaxation processes based on the drastic difference in the mechanical properties of the hard and soft segments. The dichotomy of the behavior of these segments stems from hydrogen bonding between the urea motifs, where the latter is the byproduct of the chemical reaction between an amine and isocyanate (Blourchian et al. 2021; Hsieh et al. 2019). The hydrogen bond regions are said to be mechanically stronger than the amorphous regions. Despite two decades of persistent research efforts, which culminated in a recently published edited book by Barsoum (2015), polyureas generally remain a fascinating model material for scientific investigations and technological applications.

The molecular structure of polyurea (as is the case for all polymers) depends on the constituents, where several formulations have been reported since 1948, when polyurea was first introduced, such as those reported in (Do et al. 2020; Hill and Walker 1948; Xu et al. 2014), for example. Nonetheless, the formulation based on the mixture of an amine with an isocyanate has recently emerged as the focus of continuous research (Barsoum 2015). The mechanical behavior of such formulation has been vigorously investigated at a broad range of strain rates extending from the quasi-static regime up to shock and ballistic loading scenarios (Mohotti et al. 2014; Qiao and Wu 2011; Roland et al. 2007; Sarva et al. 2007). The research demonstrated that this aromatic polyurea exhibits superior mechanical and physical properties, including ultrahigh extensibility, chemical, moisture and abrasion resistance, high adhesion strength, and remarkable impact mitigation (Bahei-El-Din et al. 2006; Grujicic et al. 2010; Youssef 2011). Collectively, these desirable engineering properties have been attributed to the segmental microstructure discussed above. For example, Roland et al. studied the effects of stoichiometric ratio (ranging from 86% to 106%) on the mechanical response of polyurea at a low strain rate of 0.06 s^{-1}. The outcomes of this study indicated that the stoichiometry-mechanical response interrelationship of polyurea is associated with the convoluted interplay of the crosslinking, interchain hydrogen bonds, and the degree of phase separation of the hard and soft domains (Roland et al. 2007). Furthermore, the segmental microstructure is thought to be responsible for a substantial increase in the interfacial strength of polyurea-based composite joints, as shown by Jain et al., reporting an interfacial strength of 370 $\pm$ 20 MPa for E-glass/polyurea composite structure compared to 198 $\pm$ 13 MPa for E-glass/epoxy counterpart (Jain et al. 2013). Jain et al. also reported that the interfacial strength for the aromatic polyurea-based structure remained nearly unchanged after exposure to harsh environmental conditions for 30 days at 50 °C and 90% relative humidity (Jain et al. 2013). Such outstanding mechanical performance is attributed to the resilience of polyurea even at high strain rates, as reported by several other researchers. For

example, Zhao et al. and Youssef et al. independently reported the dynamic tensile strength of polyurea under shock-loaded conditions, where the first group found the intrinsic tensile strength to be 106 MPa, whereas the latter reported a value of 93 $\pm$ 5 MPa (Youssef and Gupta 2011; Zhao et al. 2008). Finally, several other research groups have recently reported further enhancement to the mechanical performance (with emphasis on energy absorption) by leveraging stochastic microstructure through the foaming of polyurea (Ramirez et al. 2018; Ramirez and Gupta 2019; Reed et al. 2020; Youssef et al. 2020). At the time of this report, the contributions of the segmental microstructure to the energy absorption of polyurea foams remain mysterious, and hence the prospect of future research.

Realizing the gap in the mechanical performance of polyurea when exposed to ultraviolet radiation, since deployment is commonly outdoors, our group launched a series of investigations to assess the effects of extended exposure to ultraviolet (UV) radiation on the hyperelastic, acoustic, and viscoelastic properties of polyurea (Whitten and Youssef 2016; Youssef et al. 2018; Youssef and Whitten 2017). It is worth noting that since our initial reports, several other groups reported on the effect of extended exposure on the mechanical performance of polyurea (Che et al. 2019; Mforsoh et al. 2020). Due to photodegradation and photooxidation, the formation of a thin degraded layer appeared to protect the mechanical properties of the bulk of the samples from harmful radiation, resulting in mild changes in the aforementioned properties. Similarly, in this case (i.e., exposure to UV radiation), the segmental microstructure also played a significant role in the resulting mechanical behaviors since the extended exposure to UV radiation altered the spatial distribution of the hard segments relative to the soft matrix on the exposed surface. Blourchian et al. (2021) investigated the microstructural evolution of polyurea over 15 weeks of continuous UV exposure by mapping the distribution of the hard/soft segments using an atomic force microscope (AFM) operating in the phase mode, where the hard segment concentration was reported to be 23% after 15 weeks, increasing from 12% within the first three weeks of exposure. Furthermore, accompanying thermogravimetric analysis substantiated the observed segmental changes from the AFM-based investigations. It was found that the weight loss of the soft segment at $\sim$300 °C decreased by $>$70% after 15 weeks compared to the pyrolyzed virgin polyurea when comparing the gravimetric results of the highlighted degraded surface layer with the surface layer of pristine unexposed samples (Blourchian et al. 2021). The propensity of the aromatic compounds to absorb the photonic energy with the ultraviolet wavelength and react with the oxygen is attributed to the above-mentioned observed evolution in the properties. It is worth noting that such changes can be further mitigated through additives such as UV absorbers or pigmentations to shift the absorption band. However, since additives unintendedly alter the physical and mechanical properties of neat polymers, an emphasis was afforded to the latter to uncover their fundamental behavior. Alternatively, Sánchez-Ferrer et al. presented an elegant solution to ultraviolet sensitivity by using aliphatic isocyanates and forming the corresponding aliphatic polyureas with enhanced ultraviolet resiliency (Rull et al. 2020; Sánchez-Ferrer et al. 2010).

One of the hallmark attributes of polymers is their time-dependent properties, showing sensitivity to extended loading duration, i.e., creep (Findley et al. 1978; Youssef 2021, 2020). Under a constant load, the polymer starts to deform with rapid increase in the strain as a function of loading time (in what is also known as primary creep), followed by an increasing deformation at a constant rate in the secondary creep regime. The polymer will transition into the terminal tertiary creep region if the load continues, ending in ultimate failure. This creep response stems from the underlying viscoelastic properties, where the dependence of the mechanical behavior is highly coupled to changes in time and temperature (Lakes 2009; Youssef 2021). Therefore the creep response of polymers can either be modeled using standalone, dedicated constitutive relationships, or based on the linear or nonlinear viscoelastic

theories (Youssef 2021). In general, the time-dependent properties are associated with various relaxation processes as functions of the loading temperature with respect to the glass transition temperature. For example, in the rubbery regime (e.g., the operating temperature is higher than the glass transition), largescale chain movements amount to the resulting large deformation. The relaxation processes can also be activated by submitting the polymer to constant stress while holding it at isothermal conditions. Youssef et al. previously showed that the creep deformation of polyurea is also mildly dependent on the exposure duration to ultraviolet radiation (Youssef and Whitten 2017). Specifically, the creep strain of virgin polyurea samples after 1000 s was found to be 23% higher than UV-exposed polyurea, irrespective of the exposure duration (i.e., mild sensitivity to exposure duration once the degraded layer formed and protected the core (Shaik et al. 2020)), also exemplified by an increase in the creep modulus. However, the extent of the interdependence of the polyurea creep behavior on the segmental microstructure and loading time is ambiguous in the current literature; hence the motivation of the research leading to this report.

This research aims to elucidate the contributions of the segmental microstructure of polyurea on the time-dependent creep deformation behavior. To facilitate this objective, thin polyurea strips were subjected to a constant load for three decades of time while acquiring high-resolution digital images of the speckled surface. The resulting digital image correlation analysis provided evidence for the contributions of the microstructure to the mechanical performance of elastomeric polymer, specifically between the hard segment distribution and the time-dependent creep response of polyurea.

2 Sample preparation

Thin polyurea strips were prepared using a spin coating technique. Specifically, thin sheets were prepared by thoroughly mixing a 4:1 weight ratio (a stoichiometric ratio of 1:1) of long-chain oligomeric diamine (Versalink® P1000, AirProducts Inc.) with modified isocyanate (MDI 143L, DOW), respectively. The specific mixing ratio was selected since it results in a hyperviscoelastic behavior, yielding observable and time-dependent deformations. The diamine/isocyanate mixture was slowly stirred with a stainless-steel stick to avoid the nucleation and entrapment of air bubbles. The mixing process continued for at least 270 s, achieving a homogenous solution. The mixture was then spin-coated on a polypropylene wafer, 150 mm in diameter, at 400 rpm for 600 s. The polyurea sheets were cured at ambient conditions (23 °C and 60% relative humidity) for 7 h, followed by an additional 12 h of curing time in a heated vacuum environment at 80 °C. Upon curing, the sheets were lifted off the polypropylene wafer, and two 24 × 142 mm strips were extracted from each sheet. At least 15 measurements of the thickness of each strip were made using an ultrasound transducer (PosiTector 6000, DeFelsko), reporting an average thickness of 78.6 ± 3.6 μm. Figure 1a schematizes the fabrication procedure of the polyurea sheet and extraction of the sample strips used in the experimental investigation discussed further.

3 Experimental method

The time-dependent response of polyurea was investigated by applying a constant load while measuring the resulting creep strain. Specifically, one end of the polyurea strip was clamped, whereas the other end was magnetically suspended to a 610 g steel block, applying a constant gravity-assisted stress of 3.1–3.4 MPa for three decades in seconds (∼1800 s) to avoid

the nonlinear viscoelastic effects (Lakes 2009; Youssef 2021). It is worth noting that the internal surfaces of the clamps were roughened in cross-hatched patterns to improve the grip and avoid any slippage or unbiased loading. This configuration resulted in a gauge length of 120 mm, measured between the clamps and the magnetically suspended weight. The latter was guided between two frictionless, opposing antirotation fixtures (Fig. 1b) to ensure the uniaxiality of the load while avoiding unintended rotations of the sample upon loading when the steel mass is freely suspended. The gauge length was covered with a random speckle pattern applied using an airbrush to facilitate the digital image correlation analysis. The creep measurements, collected at ambient conditions (21 ± 0.7 °C and 41.2 ± 4.1% RH), consisted of two steps. First, several pictures of the load-free samples were captured while a spacer supported the steel block, where the spacer has a height equivalent to the distance between the experimental bench and the natural unloaded length of the sample. These preliminary images were used as the reference for the strain calculations during the DIC analysis to estimate the strain noise floor. The still image analysis resulted in strain noise orders of magnitude smaller than the actual strain during loading. Second, the spacer was carefully and gently removed to load the sample due to the weight of the suspended steel block, where digital images were concurrently collected at a frame rate of 10 fps using a digital camera (Basler, acA1300-30gc) fitted with an objective lens (HAYEAR 10-300x), resulting in a 4.9 mm × 6.5 mm field of view, a much smaller portion of the sample dimension. This process was repeated for three thin polyurea samples randomly selected from three spin-coated sheets.

The ex situ digital image correlation (DIC) analysis was used to calculate the in-plane strain components. The images were analyzed using a commercial digital image correlation software (Vic-2D, Correlated Solutions, Inc.), where the in-plane strain components were determined using subset, step, and strain filter sizes of 41 pixels (214 μm), 10 pixels (52 μm), and 5, respectively. The utilized set of image correlation parameters was selected after a sensitivity analysis whose objective was to maximize the strain-to-noise ratio (Koohbor et al. 2017), while allowing for the identification of localized strain bands developed due to the segmental deformation patterns in polyurea. Specifically, the virtual strain gage size (step size × strain filter = 260 μm) associated with the DIC parameters was small enough to characterize local strain fields and their resulting strain gradients.

The extracted spatial average strain components include the normal axial strain ε_y, normal lateral strain ε_x, in-plane shear strain ε_{xy}, and in-plane rotation ω, where the center of rotation was defined to be the center of the image field of view. In addition to the strain components, full-field strain contour maps were extracted at increments of 1 min to explicate the spatial distribution of the creep mechanical behavior of polyurea, detecting possible regions of strain localization. Since the polyurea samples underwent constant stress under isothermal conditions, the dynamic response of the axial creep strain data was fit into the Norton–Bailey law

$$\varepsilon_c = \phi \sigma^{\alpha} t^{\beta} \tag{1}$$

where, ϕ, α, and β are the parameters found by curve fitting the primary and secondary creep, independently. Equation (1) is the convolution of the Norton stress power law and the Bailey time power law, which has been demonstrated to accurately capture the creep response of polymers (Youssef 2021). Here the Norton stress power law was considered as a constant since the stress for each sample was held constant throughout the experiment, i.e., setting the Norton power to unity and plugging in the corresponding applied stress value during the regression analysis, that is, Eq. (1) is reduced to the equation

$$\varepsilon_c = \phi \sigma t^{\beta}. \tag{2}$$

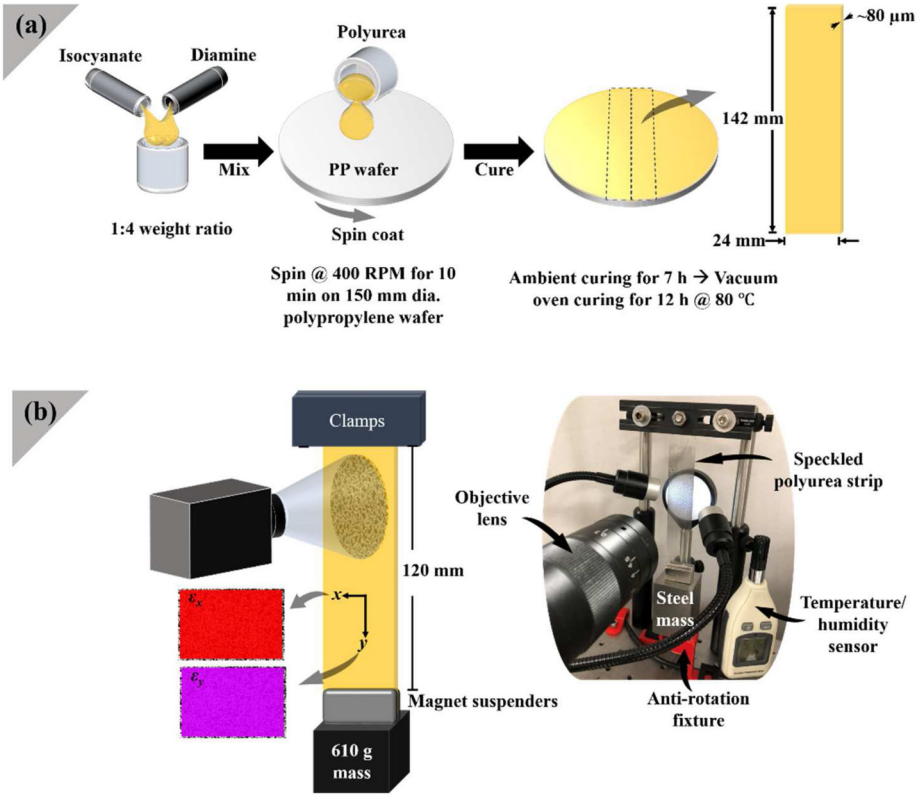

Fig. 1 Schematic of the (a) fabrication procedure of the polyurea sheets, from which the 142 × 24 mm strips were extracted to perform the (b) creep loading experiment by applying a constant stress using a magnetically suspended steel mass

In addition, the axial creep strain data were also fitted into a two-element Kelvin model (Eq. (3)), where each element consists of a spring and dashpot in parallel. The two elements were connected in series since the creep rate in the primary region differs from the secondary counterpart. The strain–stress relationship for the two-element Kelvin model is

$$\varepsilon(t) = \frac{\sigma_0}{E_1}\left(1 - \exp\left(-\frac{E_1 t}{\eta_1}\right)\right) + \frac{\sigma_0}{E_2}\left(1 - \exp\left(-\frac{E_2 t}{\eta_2}\right)\right), \tag{3}$$

where σ_0 is the applied constant stress, E_1 and E_2 are the spring constants of the first and second Kelvin elements, and η_1 and η_2 are the viscosities of the dashpots, respectively.

The preceding regression analyses hinge on identifying the transition between the primary and secondary creeps. The primary creep rate is faster than the secondary counterpart, which remains nearly constant. To delineate the transition, straight line fit subtraction was performed over the entire strain-time history using the "*detrend*" function in the Signal Processing Toolbox in MATLAB®. The subtraction magnified the ascending creep rate in the primary region and exemplified the secondary rate as a descending slope. The transition region was clearly elucidated as an inflection region.

4 Results and discussion

The time-dependent creep strain components of the polyurea samples extracted from the DIC analysis are shown in Fig. 2, exemplifying a typical creep response of elastomeric polymers. Such a creep response starts with an instantaneous jump in the strain due to the intrinsic stiffness of the material, stemming from the instantaneous elastic modulus. The axial creep strain at ~20 s (where the jump of the initial deformation fades into the next phase of the response) is 0.003 ± 0.0006, which translates into an instantaneous modulus of 1.2 ± 0.2 GPa based on the applied constant stress of 3.1–3.4 MPa. This was found to be in excellent agreement with previous reports of the instantaneous modulus of polyurea of ~1 GPa investigated by Knauss and Zhao (2007). Thereafter, the primary creep commences, where the creep strain rapidly increases at a rate of 3×10^{-5} s^{-1}, followed by a secondary creep region. The strain in the latter ascends at a nearly constant rate of 4×10^{-6} s^{-1} until the end of the loading time. The creep rates in the primary and secondary regions were calculated based on the time derivative of the Norton–Bailey law, as discussed next. It is worth reiterating that the loading time was selected to avoid the tertiary terminal creep to ensure that the field of view is not lost during the image acquisition process. The normal axial strain increased from the unloaded condition to 0.02 over the entire loading time; however, 73% of this deformation was achieved over the first 540 s. The corresponding lateral strain reached a final value of 0.008 over the same loading time. The overall trend and the final value of the creep strains reported in this experiment warrant two additional observations. First, the axial and lateral creep strains follow the same overall trend as functions of time since Poisson's ratio is generally perceived as a time-independent property for linear nearly incompressible or incompressible material, as discussed later. Poisson's ratio is associated with the volumetric deformation, further substantiating the time independence behavior since the hydrostatic deformation is isometric. Second, the final value of the axial creep strains (0.02 ± 0.002) is consistent with the results of previous research, where the latter reported 0.009 creep strain after 1200 s of loading at 20 °C, but at an applied stress of only 0.5 MPa. The dichotomy in the final strains (reported herein versus by Youssef and Whitten (2017)) is substantiated based on (1) the difference in the applied stresses (3.4 MPa versus 0.5 MPa, respectively) and (2) the nonlinearity of creep response with respect to the applied load. Furthermore, the elastic moduli are shown to be time dependent for polymers, including elastomers, due to their mechanistic connection to distortional part of the deformation process.

In addition to the normal strain components, the full-field DIC analysis revealed a measurable in-plane shear despite the uniaxially applied stress. It is important to recall that the samples were secured into roughened and fastened clamps, minimizing any induced extrinsic strains. Moreover, accompanying axial deformation with shear strain is mechanistically consistent with anisotropic or mildly anisotropic materials. Figure 2c shows the resulting in-plane shear strain as a function of the loading time, inheriting a similar temporal creep response of the normal strain components as that discussed previously within the primary and secondary creep regions. The in-plane creep shear strain (ε_{xy}) is on average ~30% of the normal lateral strain (ε_x) and ~13% of the normal axial strain (ε_y) over the entire loading history. From a mechanics perspective, the case investigated herein of thin polyurea films can be considered as a plane stress problem with a uniaxial load applied along the gauge length and can be summarized by the following stress–strain equation:

$$\begin{bmatrix} \varepsilon_x \\ \varepsilon_y \\ \varepsilon_{xy} \end{bmatrix} = \frac{1}{E} \begin{bmatrix} 1 & -\nu & 0 \\ -\nu & 1 & 0 \\ 0 & 0 & 2(1+\nu) \end{bmatrix} \begin{bmatrix} 0 \\ \sigma_y \\ 0 \end{bmatrix}, \tag{4}$$

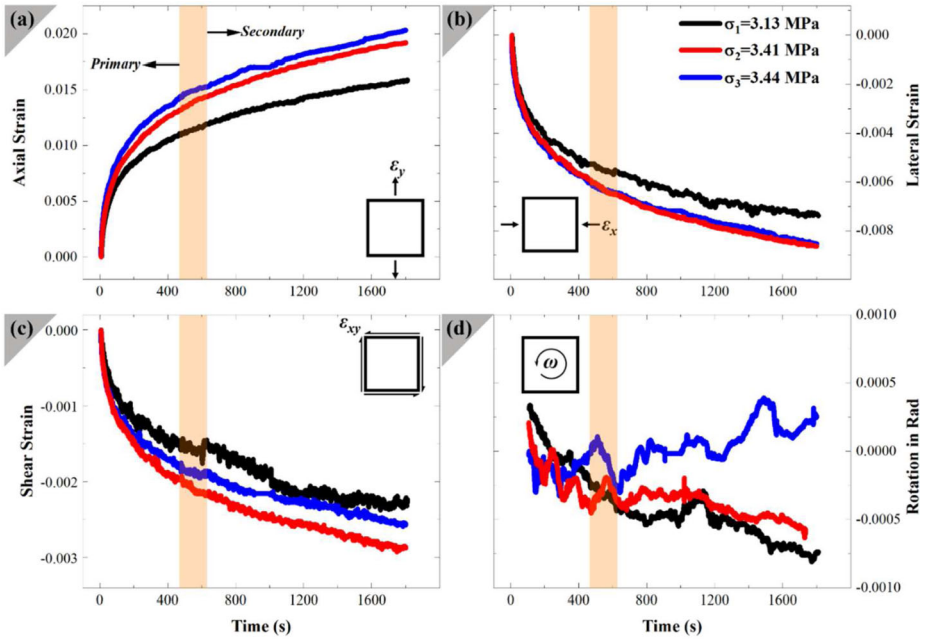

Fig. 2 Normal (a) axial and (b) lateral strain, (c) in-plane shear strain, and (d) in-plane rotation extracted from the full-field DIC analysis of three creep-loaded thin-film polyurea samples

where, σ_y is the applied axial stress, E is the elastic modulus, ν is Poisson's ratio, and ε_x and ε_y are the normal lateral and axial strains, respectively. The results from Eq. (4) differ strikingly from the experimental shear strain data. The development of creep shear strain implies creep-activated changes to the shear modulus. That is to say, the pure uniaxial loading should result in only normal axial and lateral strains (i.e., Eq. (4)). Instead, it induced an additional shear strain component as the loading time increased. Such changes in the shear stiffness of the material can be explained by considering two fundamental mechanisms. First, the generated shear strain is nearly negligible (compared to the accompanying axial components) at the onset of the measurement but persistent at comparable levels between samples. Here the creep shear strain is 0.0004, whereas ε_y and ε_x are 0.003 and 0.001, respectively, at the 20 s mark, delineating the end of the initial deformation, indicating the consistency between the uniaxial applied load and the mechanistically forecasted state of deformation as described by Eq. (4). However, the shear strain becomes a major player in the state of deformation as time lapses, exemplifying an underlying shear softening phenomenon, the second fundamental mechanism. At the end of the loading, the final shear strain was up to 0.0028, decreasing at a rate of 5×10^{-7} s^{-1} in the secondary creep region. The shear softening phenomenon is an interplay between the sense of the axial loading, i.e., being tensile, and the macromolecule mobilities. On the one hand, the tensile load induces a deformation due to stretching, uncoiling, and largescale sliding between the polymer chains to accommodate the intensity of the load, resulting in a reduction in the shear stiffness of the material. On the other hand, the long-term loading associated with creep acts as a temporal plasticization agent that also gives way to largescale molecular motions. This is a strain aging effect (Findley et al. 1978; Youssef 2021). The combination of these mechanisms results in the reported creep-activated shear softening behavior of polyurea, allowing for enhanced energy dissi-

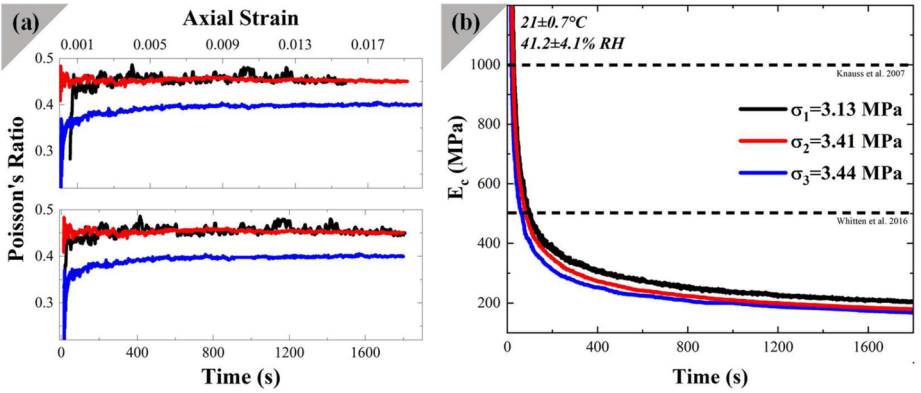

Fig. 3 Calculated (a) Poisson's ratio based on the extracted full-field lateral and strain components and (b) elastic modulus based on the in-plane strain and constant applied stress of each corresponding polyurea sample

pation in realistic loading scenarios, a known attribute of this fascinating material. In other words, the creep-activated reduction in the shear stiffness of the material is associated with a reversible anisotropy based on the interaction of the applied load with the segmental microstructure of polyurea, as discussed later. It is imperative to note that the negligible levels of in-plane rotations (as shown in Fig. 2d) further substantiate the aforementioned mechanisms by demonstrating that the resulting state of deformation is consistent with the applied uniaxial load and the creep-activated softening behavior. It is worth noting that other chemo-mechanical factors may also be playing a role in the overall behavior of the materials, which is a topic for future research.

Figure 3 shows the extracted mechanical properties based on the full-field strain measurements using the DIC analysis, where Fig. 3a is a plot of Poisson's ratio as a function of time on the bottom panel of the figure and as a function of axial creep strain on the top panel. After the initial period (i.e., < 20 s), Poisson's ratio appears to be time-insensitive, with a value of 0.43 ± 0.03 for the remaining loading time. The time invariability of Poisson's ratio is attributed to the similarities in the temporal creep behavior of the lateral and axial strains. That is to say, the near-identical creep behaviors of the axial and lateral creep strains in the primary and secondary creep regions substantiate the constant Poisson ratio and the compatibility of the deformation mechanisms in the axial and lateral directions. It is worth noting that the value of Poisson's ratio reported herein (~ 0.43) differs from that reported before by Knauss et al. ($\nu = 0.486$), where the difference is associated with the different testing mechanisms and the corresponding strain rates. On the other hand, the creep modulus plotted in Fig. 3b is time dependent, as expected, since it was calculated by dividing the resulting creep axial strain by the constant applied stress. The time-dependent behavior of the elastic modulus is consistent with the viscoelastic behavior of polyurea, as demonstrated by various researchers over the past few years. The time variability of the creep modulus is also rooted in the creep-activated relaxation processes previously discussed. In essence, the time-independent behavior of Poisson's ratio is attributed to its inherent near-incompressibility, whereas the time-dependent creep modulus is associated with its viscoelastic behavior. This paradoxical behavior has been explicated when applying the linear viscoelastic theory to polyurea, where the relaxation processes are generally attributed to the deviatoric deformation while the volumetric contributions are linearly elastic (Knauss and Zhao 2007). In other

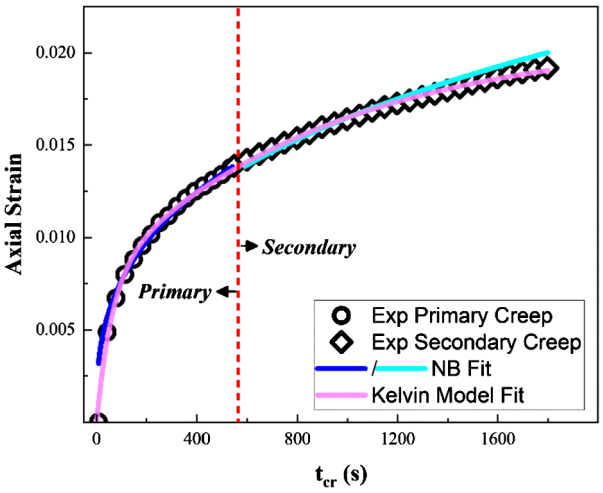

Fig. 4 Representative of the piecewise fitting of the in-plane axial strain with the Norton–Bailey equation, where the correlation coefficient between the fitted and the experimental data for both the primary and secondary creeps were found to be 0.99

Table 1 Summary of the parameters based on the fitting of the primary and secondary creeps of the load polyurea strips using the Norton–Bailey law (2) and the two-element Kelvin model (3), where σ_1 (3.13 MPa), σ_2 (3.41 MPa), and σ_3 (3.44 MPa) correspond to the applied stresses of the three tested samples

Model Parameter	σ_1		σ_2		σ_3	
	Primary	Secondary	Primary	Secondary	Primary	Secondary
ϕ	0.021	0.00069	0.0041	0.00072	0.0057	0.00084
β	0.036	0.27	0.13	0.27	0.11	0.26
E_1 (MPa)	458		436		385	
η_1 (MPa s)	27400		26980		22040	
E_2 (MPa)	300		262		268	
η_2 (MPa s)	287500		239000		249000	

words, the time-dependent behavior of incompressible polyurea within the realm of linear viscoelasticity is always captured by the distortional component of the strain state due to the dependence of the modulus on time while the hydrostatic component remains time invariant, as discussed before. However, it is important to note that this is not applicable to compressible viscoelastic materials (Findley et al. 1978), which might be the case for other polyurea variants (Sánchez-Ferrer et al. 2021, 2015, 2010).

As mentioned before, the axial creep strain-time history was fitted into the Norton–Bailey law, where the primary and secondary creeps were fitted independently due to the difference in the creep rate. Representative fitting parameters, on average, for the primary creep region include $\phi = 0.01$ MPa^{-1} s$^{-\beta}$ with $\beta = 0.09$. As demonstrated in Fig. 4, the Norton–Bailey law accurately fitted the data with a correlation coefficient >0.98 for the primary creep region. Similarly, the fitting parameters for the secondary creep are $\phi = 7.5 \times 10^{-4}$ PMPa^{-1} s$^{-\beta}$ with $\beta = 0.26$ with comparable levels of the goodness of the fit, on average. The remaining results of the Norton–Bailey fittings are succinctly summarized in Table 1. The fitting parameters listed in Table 1 are consistent between all the samples, irrespective of the slight differences in the applied stresses, while reiterating that the strip samples were extracted from different spin-coated polyurea sheets. The fitting consistency highlights the reproducibility of the spin coating process, judged by the repeatability of

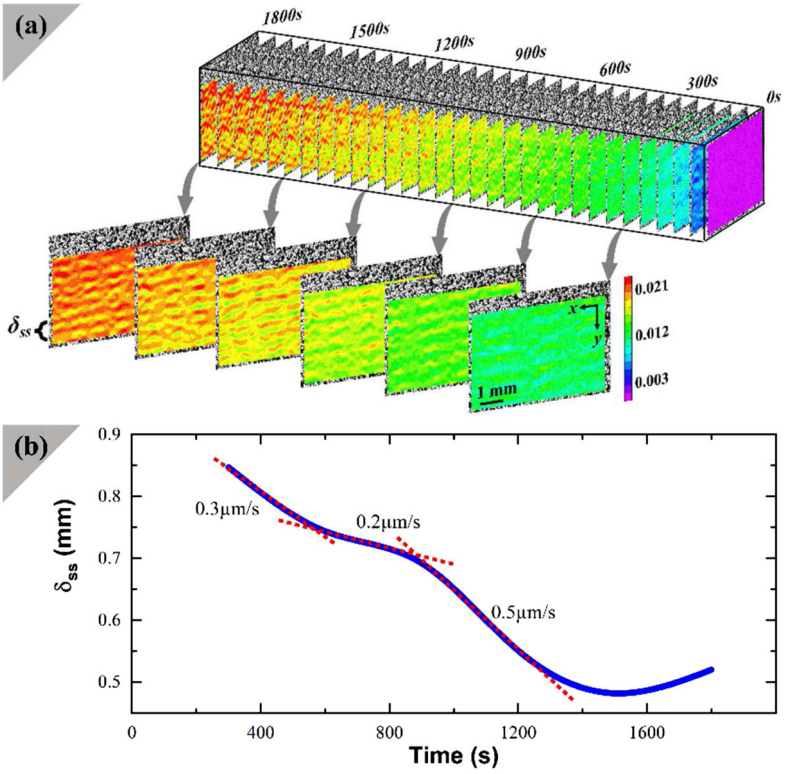

Fig. 5 (a) Creep axial strain contour maps extracted at 1 min increments, where δ_{ss} is the distance between subsequent areas of high strains. (b) Plot of δ_{ss} as a function of time, where three distinct linear regions, attributed to the responses of the segregated hard and soft segments, can be seen

the thickness and mechanical behavior from one batch to another. It also demonstrates that there exist two distinct relaxation processes within the primary and secondary creep regions, where the fitting parameters in these regions are distinctly different but remarkably similar between the samples. Generally, these relaxation processes exhibit higher dependency on time based on the fitted values of β while noting the difference in the fitting parameters within the primary and secondary creeps. The time power exponent β was <1, indicating the occurrence of strain softening, which is expected for creep loading. Notably, the primary region is accompanied by the high resistance to deformation as exhibited in Fig. 3b, where the primary creep elastic modulus was found to be much larger than that seen in the secondary creep. It is also consistent with the rapid creep rate in the primary creep. Moreover, the low secondary creep viscosity validates the analysis of the creep-activated shear softening behavior discussed above, in which a more fluid-like mobility (i.e., largescale deformation in a solid) shears easily.

Figure 4 and Table 1 also include the results from fitting the axial creep strain data into a classical two-element Kelvin model (2). Here the entire creep history was fitted simultaneously into the model using nonlinear least-squares regression, yielding a correlation coefficient > 0.99. The drastic difference between the fitting parameters in the first and second Kelvin elements implies two distinct molecular processes. Generally, the stiffness of the first element is higher than the second element, whereas the viscosity values are higher

for the second element than those for the first element. The high stiffness and low viscosity in the first creep process, i.e., the first Kelvin element, indicate that the significant chain mobility dominated the creep response, embodied in the rapid increase in the creep strain within the initial 300 s. The substantial increase in viscosity in the second Kelvin element ($\eta_2 \gtrsim 10\eta_1$) implies that deformation-resistant processes are more prevalent subsequently after the contributions of the first element diminish.

Figure 5a shows a series of contour plots of the axial creep strain as a function of loading time based on full-field strain analysis using the DIC approach with emphasized panels (contour plots laid over optical speckled images) extracted at an increment of 300 s. The strain contour plots demonstrate a twofold character of the state of deformation, namely, the progressive and nonuniform state of creep strain as the loading time lapsed. The progressive aspect has been discussed a priori, where the creep strain increases as a function of time (e.g., Fig. 4) while the applied stress was kept constant. The nonuniform behavior of the axial creep strain was absent from the previous discussion since the extraction necessitates averaging over the region of interest, which was taken to be the entire picture frame. This nonuniform distribution persisted in all tested samples and exhibited nearly the same evolution, where areas of high strains spring into the contour plots surrounded by regions of inferior strains. The high strain regions develop into continuous striations perpendicular to the loading direction across the contours. These striations are thought to be associated with the segmental microstructure of polyurea consisting of hard domains within soft segments with different mechanical properties (Blourchian et al. 2021; Choi et al. 2012). Atomic force microscope studies previously showed a drastic contrast between the soft and hard domains due to differences in their mechanical properties, where the hard segments were shown to be brighter than their soft counterpart (Blourchian et al. 2021). Thus the segmental microstructure responds to mechanical loads by activating relaxation processes from the hard and soft domains based on the generated creep strain and applied stress (i.e., strain energy). As mentioned above, the latter is characterized by higher compliance than the former, resulting in strain localization within the soft regions as exemplified in the contour plots in Fig. 5a. The striations separation distance δ_{ss} was measured from the contour plots of the axial strain as a function of time, plotted in Fig. 5b. The extracted striations separation can be divided into three regions elucidating different relaxation mechanisms were activated by the creep strain history.

The first relaxation mechanism is within the primary creep with the striations separating at a rate of 0.3 μm/s followed by two relaxation processes in the secondary creep. In the primary region the relaxation process is due to an interplay between the strain-induced mobility of the soft and hard segments, where such convoluted response can only be resolved with nanoscale strain measurements, which are beyond the scope of the current study but are a topic of future research endeavors. On the other hand, the relaxation processes within the secondary creep are sequentially attributed to the hard and soft domains. The relaxation of the hard domains, physically linked through weak hydrogen bonds, occurred within 600–850 s with a striation separation rate of 0.2 μm/s. The soft domains (along the main chain of the polyurea monomer) showed another distinct relaxation process after that attributed to the hard segments at a rate of 0.5 μm/s for the latter. The rationale for assigning the lower separation rate to the hard segment arises from their higher stiffness reported previously using an atomic force microscope (Blourchian et al. 2021). The faster rate is associated with the soft domain given their inferior elastic properties based on the Cox–Merz relationship, the low-viscous segment in polyurea, as a function of time varied between primary and secondary creeps. Therefore the DIC analysis provided evidence for the contributions of the segmental microstructure to the overall mechanical performance of polyurea by revealing distinct relaxation processes in the primary and secondary creep regions.

5 Conclusion

DIC analysis was used to delineate the full-field creep strain response of thin-film polyurea, a thermoset elastomer, submitted to constant stress for three decades. The mechanical behavior of polyurea is hyperviscoelastic, i.e., dependent on loading rate and temperature. High-resolution digital images of loaded polyurea strips speckled with a randomized pattern were collected and analyzed to extract the in-plane strain components as functions of loading time. The full-field analysis reveals the creep strain in the axial, lateral, and in-plane shear directions when stress of 3.1–3.4 MPa was constantly applied for 1800 s, denoting primary and secondary creep regions and exemplifying the time-dependent behavior of the polymer. Remarkably, the presence of a measurable shear strain, despite a uniaxial loading condition, demonstrates a shear softening phenomenon and elastic anisotropy under creep-loaded conditions. The resolved Poisson ratio remained nearly constant throughout the loading time, supporting the inherent incompressibility of the material and time-independence of the property. On the other hand, the time-dependent behavior of the elastic creep modulus is linked to the viscoelastic property of polyurea elastomer. Together, these mechanisms validate that creep response can be modeled using linear viscoelasticity, where the volumetric deformation captures the time-independent incompressible attributes of polyurea elastomer, whereas the deviatoric deformation is attributed to the time-dependent elastic properties. Finally, the extraction of contour maps from the DIC full-field strain analysis revealed different molecular transitions as functions of loading time, where specific relaxation mechanisms were linked to the segregated hard and soft segmental microstructure of polyurea. Therefore the outcomes of this research provided physical evidence for the particular contributions of the segmental microstructure to the overall mechanical behavior of elastomeric polyurea.

Acknowledgements The research leading to these results was supported in part by the United States Department of Defense under Grant Agreement No. W911NF1410039 and W911NF1810477. The National Science Foundation under Award No. 1925539 also supported the research. The authors are also grateful for internal funding from San Diego State University.

Declarations

Competing Interests The authors declare no competing interests.

References

Bahei-El-Din, Y.a., Dvorak, G.J., Fredricksen, O.J.: A blast-tolerant sandwich plate design with a polyurea interlayer. Int. J. Solids Struct. **43**, 7644–7658 (2006). https://doi.org/10.1016/j.ijsolstr.2006.03.021

Barsoum, R.G. (ed.): Elastomeric Polymers with High Rate Sensitivity Elsevier, Oxford (2015)

Blourchian, A., Shaik, A.M., Huynh, N.U., Youssef, G.: Segmental evolution of ultraviolet weathered polyurea. J. Polym. Res. **28**, 117 (2021). https://doi.org/10.1007/s10965-021-02483-4

Che, K., Lyu, P., Wan, F., Ma, M.: Investigations on aging behavior and mechanism of polyurea coating in marine atmosphere. Materials **12**, 3636 (2019). https://doi.org/10.3390/ma12213636

Choi, T., Fragiadakis, D., Roland, C.M., Runt, J.: Microstructure and segmental dynamics of polyurea under uniaxial deformation. Macromolecules **45**, 3581–3589 (2012). https://doi.org/10.1021/ma300128d

Do, S., Stepp, S., Youssef, G.: Quasi-static and dynamic characterization of polyurea microspheres reinforced polyurea matrix composite. Mater. Today Commun. **25**, 101464 (2020). https://doi.org/10.1016/j.mtcomm.2020.101464

Findley, W.N., Lai, J.S., Onaran, K.: Creep and Relaxation of Nonlinear Viscoelastic Materials. Dover, New York (1978)

Grujicic, M., Pandurangan, B., He, T., Cheeseman, B.A., Yen, C.F., Randow, C.L.: Computational investigation of impact energy absorption capability of polyurea coatings via deformation-induced glass transition. Mater. Sci. Eng. A **527**, 7741–7751 (2010). https://doi.org/10.1016/j.msea.2010.08.042

Gupta, V., Crum, R., Gamez, C., Ramirez, B., Le, N., Youssef, G., Citron, J., Kim, A., Jain, A., Misra, U.: Adhesive and ultrahigh strain rate properties of polyurea under tension, tension/shear, and pressure/shear loadings with applications to multilayer armors. In: Elastomeric Polymers with High Rate Sensitivity: Applications in Blast, Shockwave, and Penetration Mechanics, Oxford (2015)

Hill, R., Walker, E.E.: Polymer constitution and fiber properties. J. Polym. Sci. **3**, 609–630 (1948). https://doi.org/10.1002/pol.1948.120030501

Hsieh, A.J., Champagne, V.K., Kooi, S.E., Schuh, C.A.: Progress on Zirconia-Polyurea Matrix Hybrid Composites. (2019)

Huynh, N.U., Gamez, C., Youssef, G.: Spectro-microscopic characterization of elastomers subjected to laser-induced shock waves. Macromol. Mater. Eng. **307**, 2100506 (2021). https://doi.org/10.1002/mame.202100506

Jain, A., Youssef, G., Gupta, V.: Dynamic tensile strength of polyurea-bonded steel/E-glass composite joints. J. Adhes. Sci. Technol. **27**, 403–412 (2013). https://doi.org/10.1080/01694243.2012.705545

Knauss, W.G., Zhao, J.: Improved relaxation time coverage in ramp-strain histories. Mech. Time-Depend. Mater. **11**, 199–216 (2007). https://doi.org/10.1007/s11043-007-9035-4

Koohbor, B., Ravindran, S., Kidane, A.: Experimental determination of representative volume element (RVE) size in woven composites. Opt. Lasers Eng. **90**, 59–71 (2017). https://doi.org/10.1016/j.optlaseng.2016.10.001

Lakes, R.: Viscoelastic Materials. Cambridge University Press, New York (2009)

Mforsoh, I.N., LeBlanc, J., Shukla, A.: Constitutive compressive behavior of polyurea with exposure to aggressive marine environments. Polym. Test. **85**, 106450 (2020). https://doi.org/10.1016/j.polymertesting.2020.106450

Mohotti, D., Ali, M., Ngo, T., Lu, J., Mendis, P.: Strain rate dependent constitutive model for predicting the material behaviour of polyurea under high strain rate tensile loading. Mater. Des. **53**, 830–837 (2014). https://doi.org/10.1016/j.matdes.2013.07.020

Qiao, J., Wu, G.: Rate-dependent tensile behavior of polyurea at low strain rates. Int. J. Polym. Anal. Charact. **16**, 290–297 (2011). https://doi.org/10.1080/1023666X.2011.587944

Raman, S.N., Ngo, T., Lu, J., Mendis, P.: Experimental investigation on the tensile behavior of polyurea at high strain rates. Mater. Des. **50**, 124–129 (2013). https://doi.org/10.1016/j.matdes.2013.02.063

Ramirez, B.J., Gupta, V.: Energy absorption and low velocity impact response of open-cell polyurea foams. J. Dyn. Behav. Mater. **5**, 132–142 (2019). https://doi.org/10.1007/s40870-019-00192-0

Ramirez, B.J., Misra, U., Gupta, V.: Viscoelastic foam-filled lattice for high energy absorption. Mech. Mater. **127**, 39–47 (2018). https://doi.org/10.1016/j.mechmat.2018.08.011

Reed, N., Huynh, N.U., Rosenow, B., Manlulu, K., Youssef, G.: Synthesis and characterization of elastomeric polyurea foam. J. Appl. Polym. Sci. **137**, 1–8 (2020). https://doi.org/10.1002/app.48839

Roland, C.M., Twigg, J.N., Vu, Y., Mott, P.H.: High strain rate mechanical behavior of polyurea. Polymer **48**, 574–578 (2007). https://doi.org/10.1016/j.polymer.2006.11.051

Rull, N., Sánchez-Ferrer, A., Frontini, P.M.: Deformation behavior of crosslinked polyurea elastomers obtained via sol-gel chemistry: experimental determination and constitutive modelling. eXPRESS Polym. Lett. **14**, 663–672 (2020). https://doi.org/10.3144/expresspolymlett.2020.54

Sánchez-Ferrer, A., Rogez, D., Martinoty, P.: Synthesis and characterization of new polyurea elastomers by Sol/Gel chemistry. Macromol. Chem. Phys. **211**, 1712–1721 (2010). https://doi.org/10.1002/macp.201000117

Sánchez-Ferrer, A., Rogez, D., Martinoty, P.: Influence of the degree of polymerisation and of the architecture on the elastic properties of new polyurea elastomers. RSC Adv. **5**, 6758–6770 (2015). https://doi.org/10.1039/c4ra09879j

Sánchez-Ferrer, A., Soprunyuk, V., Engelhardt, M., Stehle, R., Gilg, H.A., Schranz, W., Richter, K.: Polyurea networks from moisture-cure, reaction-setting, aliphatic polyisocyanates with tunable mechanical and thermal properties. ACS Appl. Polym. Mater. **3**, 4070–4078 (2021). https://doi.org/10.1021/acsapm.1c00578

Sarva, S.S., Deschanel, S., Boyce, M.C., Chen, W.: Stress-strain behavior of a polyurea and a polyurethane from low to high strain rates. Polymer **48**, 2208–2213 (2007). https://doi.org/10.1016/j.polymer.2007.02.058

Shaik, A.M., Huynh, N.U., Youssef, G.: Micromechanical behavior of ultraviolet-exposed polyurea. Mech. Mater. **140**, 103244 (2020). https://doi.org/10.1016/j.mechmat.2019.103244

Wang, Y., Zhou, X., Lin, M., Zhang, Q.M.: High-energy density in aromatic polyurea thin films. Appl. Phys. Lett. **94**, 202905 (2009). https://doi.org/10.1063/1.3142388

Whitten, I., Youssef, G.: The effect of ultraviolet radiation on ultrasonic properties of polyurea. Polym. Degrad. Stab. **123**, 88–93 (2016). https://doi.org/10.1016/j.polymdegradstab.2015.11.009

Xu, J., Han, H., Zhang, L., Zhu, X., Jiang, X., Kong, X.Z.: Preparation of highly uniform and crosslinked polyurea microspheres through precipitation copolymerization and their property and structure characterization. RSC Adv. **4**, 32134–32141 (2014). https://doi.org/10.1039/c4ra04206a

Youssef, G.: Dynamic Properties of Polyurea (2011)
Youssef, G.: Creep analysis of E-glass/vinyl-ester laminated composites for underground vault structures. Polym. Compos. **41**, 3564–3574 (2020). https://doi.org/10.1002/pc.25643
Youssef, G.: Applied Mechanics of Polymers. Elsevier, Amsterdam (2021)
Youssef, G., Gupta, V.: Dynamic tensile strength of polyurea. J. Mater. Res. **27**, 494–499 (2011). https://doi.org/10.1557/jmr.2011.405
Youssef, G., Whitten, I.: Dynamic properties of ultraviolet-exposed polyurea. Mech. Time-Depend. Mater. **21**, 351–363 (2017). https://doi.org/10.1007/s11043-016-9333-9
Youssef, G., Brinson, J., Whitten, I.: The effect of ultraviolet radiation on the hyperelastic behavior of polyurea. J. Polym. Environ. **26**, 183–190 (2018). https://doi.org/10.1007/s10924-016-0933-x
Youssef, G., Reed, N., Huynh, N.U., Rosenow, B., Manlulu, K.: Experimentally-validated predictions of impact response of polyurea foams using viscoelasticity based on bulk properties. Mech. Mater. **148**, 103432 (2020). https://doi.org/10.1016/j.mechmat.2020.103432
Zhao, J., Knauss, W.G., Ravichandran, G.: Applicability of the time–temperature superposition principle in modeling dynamic response of a polyurea. Mech. Time-Depend. Mater. **11**, 289–308 (2008)